RADLER - A UNICYCLE AS A LOW-COST RADIAL LASER SCANNER

Dorit Borrmann*, Sven Jörissen, Andreas Nüchter

Informatics VII – Robotics and Telematics, Julius Maximilian University of Würzburg, Germany
{dorit.borrmann|sven.joerissen|andreas.nuechter}@uni-wuerzburg.de

Commission I, WG I/7

ABSTRACT:

In recent years a wide range of 3D multi sensor systems for various applications has been proposed. Each of them has its own benefits and limitations. This paper proposes a modified unicycle with a 2D laser profiler attached to the wheel axle, thus creating a radial 3D scanning pattern. This novel low-cost device combines the advantages of wheeled scanning equipment with those of wearable or hand-held devices. After presenting the hardware setup and the sensor integration, the results are evaluated using four test scenarios and a terrestrial laser scanner for comparison.

1. INTRODUCTION

In recent years, optical 3D measurement devices have undergone a rapid development. With increased speed and accuracy on the one hand and decreased weight and hardware costs on the other hand they are on the way of becoming the standard measurement tool in many disciplines. Naturally, different measuring principles come with different advantages and disadvantages, depending on the area of application. For measuring large areas in a timely manner mobile scanning solutions are the method of choice. Laser scanners as well as camera systems mounted on cars, trolleys, backpacks or aerial vehicles have been developed depending on specific requirements.

Mobile mapping systems consisting of sensors mounted on cars are the state of the art for mapping urban environments. However, they are limited to areas that are accessible by car. Robotic solutions (Nüchter et al., 2013) or solutions with scanners mounted on carts, like the VIAmetris iMMS (VIAmetris, 2015, Thomson et al., 2013), the Google Street View Trolley (Google, 2015), or the NavVis 3D Mapping Trolley (NavVis, 2015) are applicable in smaller alleys. At stairs as well as dirt or gravel roads these systems still meet their limits. Airborne laser scanning is not restricted to specific terrain and thus has advantages, but it is not available in roofed environments or tunnels or gives unsatisfying results in areas with a lot of trees or bushes. Backpack mounted systems, also known as personal laser scanning, such as "The Cartographer" by Google (Frederic Lardinois, TC, 2015), the Zebedee 3D sensor system (Bosse et al., 2012), the Leica Pegasus:Backpack (Leica, 2015) or our own backpack mobile mapping system (Lauterbach et al., 2015), have been presented as ideal solutions to overcome these issues for indoor mapping. While all of them perform great for said requirements and tasks, all come with disadvantages such as high weight of the backpack, high hardware costs or low range (Zebedee 3D, 15-30 m).

A different approach was recently presented in form of the "Classical Mechanics Scanner" (Lehtola et al., 2015) and extended in (Lehtola et al., 2016). Although it is simple and easy to operate, steering the wheel is not possible since the localization is only performed in an intrinsic manner, which requires a straight the path. Additionally, it needs to be regularly pushed

Figure 1. First author operating RADLER[1] (RADial LasER scanning device).

for a continuous movement, making the operation exhausting for long scans. Therefore, the field of application is very limited, especially considering challenging and rough terrain.

While camera systems meet their limits in changing lighting conditions and featureless environments, the main drawback of full 3D laser scanners is still the respectable price range and the weight. Inspired by the concept of a surveyor's wheel, this paper continues the work on a low-cost 3D scanning solution, RADLER[1] (a RADial LasER scanning device), that consists of a 2D laser scanner mounted on the axle of a unicycle (cf. Fig. 1), first presented in (Borrmann et al., 2018). The wheel rotation creates a radial 3D scanning pattern. Moving on the ground leads to a smoother trajectory than handheld or backpack systems. Nevertheless, with the large pneumatic wheel, RADLER can be operated on rough terrain and

---

* Corresponding author

[1] https://en.wikipedia.org/wiki/Shandy#Radler

even stairs if the operator stands above the wheel. Additionally, with about 9 kg it is lightweight, highly portable and easy to operate. Ideal applications are surveying and mapping in small, narrow areas where precise reconstruction of small features is not the main objective. To create the 3D scan pattern, a rotary encoder and an inertial measurement unit (IMU) are used. The SLAM algorithm (Simultaneous Localization and Mapping) (Elseberg et al., 2013) is then applied to calculate the final point cloud from initial data. The scientific contribution of this paper is an improved data processing pipeline, that is demonstrated on a challenging real-world data set.

After a technical overview, four real world experiments are presented and compared to data acquired with a terrestrial 3D laser scanner. The results show high precision in generated floor planes of indoor and outdoor data. Most measurement errors lie within 20 cm. Since all sensors are mounted relatively low above ground, outdoor experiments with long, straight trajectories yield a high deviation on the edges of the data sets in the recorded elevation profile which is prone to be amplified in the SLAM alignment. The improved data processing pipeline presented here leads to better initial poses reducing this effect.

2. TECHNICAL APPROACH

RADLER is a low-cost scanning device that combines the advantages of wheeled 3D measurement equipment with those of hand-held or wearable devices. It consists of a modified unicycle with an attached handle for easy maneuverability, as seen in Fig. 1. It is light-weight and moves smoothly on the ground due to the large pneumatic wheel, which also allows it to be used in rough terrain and even on stairs, when the operator is rather pulling than pushing.

2.1 Hardware setup

The sensors, namely a SICK LMS141 LiDAR sensor, a PhidgetSpatial Precision 3/3/3 IMU, a Raspberry Pi 3 single board computer (SBC) with display and a Phidget rotary encoder ISC3004, are mounted on a base plate that is connected to the wheel axle as seen in Fig. 2. Counterweights on the other side help to keep the wheel in balance during operation. For best stability, the weights move the center of gravity onto the wheel (cf. red line in Fig. 2(b)). The rotary encoder is fixed with respect to the unicycle frame via a support structure and connected via the PhidgetEncoder High Speed to the SBC through USB. A coupler releases the axial stress from the encoder during rotation. The LMS141 with a maximum operating range of 40 m at a scanning frequency of 25/50 Hz and resolution of 0.25 / 0.5 ° is mounted with its scanning plane parallel to the wheel axle and connected to the SBC via Ethernet. While other LiDARs have been considered, namely Velodyne PUCK (worse angular resolution and accuracy) and Livox Mid-40/Mid-100 (worse horizontal FOV), the LMS141 has been chosen as it provides the best price-performance ratio. The Raspberry Pi 3 is configured as a WiFi access point, such that easy communication via *ssh* is possible. The wheel encoder is used for simple odometry and later on fused with the IMU to get a precise trajectory. RADLER is powered through a 11.1 V 1000 mAh lithium polymer battery, that allows and operation time of about 40 to 50 min and is also directly mounted on the base plate, giving 11.1 V for the laser scanner and 5 V via a DC-DC converter for the SBC.

2.2 Sensor integration

The Raspberry Pi 3 integrates the sensors using ROS (the Robot Operating System). The laser scanner rotates around the wheel axis to create a radial 3D point cloud while moving forward at the same time. This ensures multiple measurements between full 360 degree rotations to provide enough overlapping data needed by the continuous-time SLAM algorithm from (Elseberg et al., 2013). The quality of the resulting 3D point cloud is thus heavily dependent on the quality of the laser scanner pose when unrolling the 2D scan slices.

The coordinate systems for RADLER are depicted in Fig 2(a). Let the unicycle coordinate system $\mathcal{U}$ be located in the center of the axis with x pointing forwards, z pointing upwards and y pointing towards the wheel through the sensor plate. The laser scanner coordinate system $\mathcal{L}$ has its origin inside the head of the scanner with x pointing towards the viewer, y pointing forwards and z pointing upwards. The IMU coordinate system $\mathcal{I}$ has its x pointing backwards, y upwards and z towards the wheel through the sensor plate. Let the global coordinate system $\mathcal{G}$ be identical to $\mathcal{U}$ at the beginning of a trajectory, where the start configuration is equal to the configuration depicted in 2(a), top, with all coordinate system being parallel to the floor.

In the following, 4x4 homogeneous transformation matrices $\boldsymbol{T}$, consisting of a 3x3 rotation matrix $\boldsymbol{R}$ and a 3x1 translation vector $t = \begin{pmatrix} x & y & z \end{pmatrix}^T$ are used:

$$\boldsymbol{T} = \begin{pmatrix} & & & x \\ & \boldsymbol{R} & & y \\ & & & z \\ 0 & 0 & 0 & 1 \end{pmatrix} = \begin{pmatrix} c\vartheta c\psi & -c\varphi s\psi + s\varphi s\vartheta c\psi & s\varphi s\psi + c\varphi s\vartheta c\psi & x \\ s\vartheta c\psi & c\varphi s\psi + s\varphi s\vartheta s\psi & -s\varphi c\psi + c\varphi s\vartheta s\psi & y \\ -s\vartheta & s\varphi c\vartheta & c\varphi c\vartheta & z \\ 0 & 0 & 0 & 1 \end{pmatrix} \quad (1)$$

with φ as roll (rotation around x), ϑ as pitch (rotation around y) and ψ as yaw (rotation around z) and s and c standing for sin and cos, respectively.

Let $\boldsymbol{T}_{\mathcal{L} \to \mathcal{U}}$ be the transformation from $\mathcal{L}$ into $\mathcal{U}$ and $\boldsymbol{T}_{\mathcal{U} \to \mathcal{G}}$ be the transformation from $\mathcal{U}$ into $\mathcal{G}$. The initial transformation of each point $\boldsymbol{p}_L$ in scanner coordinates into the global coordinate system is then calculated as

$$\boldsymbol{p}_G = \boldsymbol{T}_{\mathcal{U} \to \mathcal{G}} \cdot \boldsymbol{T}_{\mathcal{L} \to \mathcal{U}} \cdot \boldsymbol{p}_L. \quad (2)$$

Let L be the circumference of the tire, and C the counts per revolution, i.e., the encoder count for a full $360°$ wheel rotation, then the change in pitch angle $\Delta\vartheta$ of the unicycle and the forward movement $\Delta x_{\mathcal{U}}$ of the unicycle are determined from the wheel encoder counts c_t between time steps $t-1$ and t as

$$\Delta\vartheta = \frac{-2\pi}{C} \cdot c_t \quad \text{and} \quad \Delta x_{\mathcal{U}} = \frac{L}{C} \cdot c_t. \quad (3)$$

IMUs are prone to drifting effects. To reduce the impact of the drift on the map quality, only the yaw ψ and roll φ angles are considered. Let $\boldsymbol{R}_{\mathcal{I} \to \mathcal{G}}$ describe the orientation of the IMU in the global coordinate system, then

$$\begin{pmatrix} p_x & p_y & p_z \end{pmatrix} = \boldsymbol{R}_{\mathcal{I} \to \mathcal{G}} \cdot \begin{pmatrix} 0 & 0 & 1 \end{pmatrix}^T \quad (4)$$

describes the z-axis of $\mathcal{I}$ in the global coordinate system. Thus the orientation of the unicycle is determined as

$$\psi = \text{atan2}(p_y, p_x) \text{ and } \varphi = \angle \begin{pmatrix} p_x & p_y & p_z \end{pmatrix}, \begin{pmatrix} p_x & p_y & 0 \end{pmatrix}, \quad (5)$$

where φ describes the angle of the vector $\begin{pmatrix} p_x & p_y & p_z \end{pmatrix}$ and its

(a) Sensor plate   (b) Center of gravity   (c) Wheel encoder
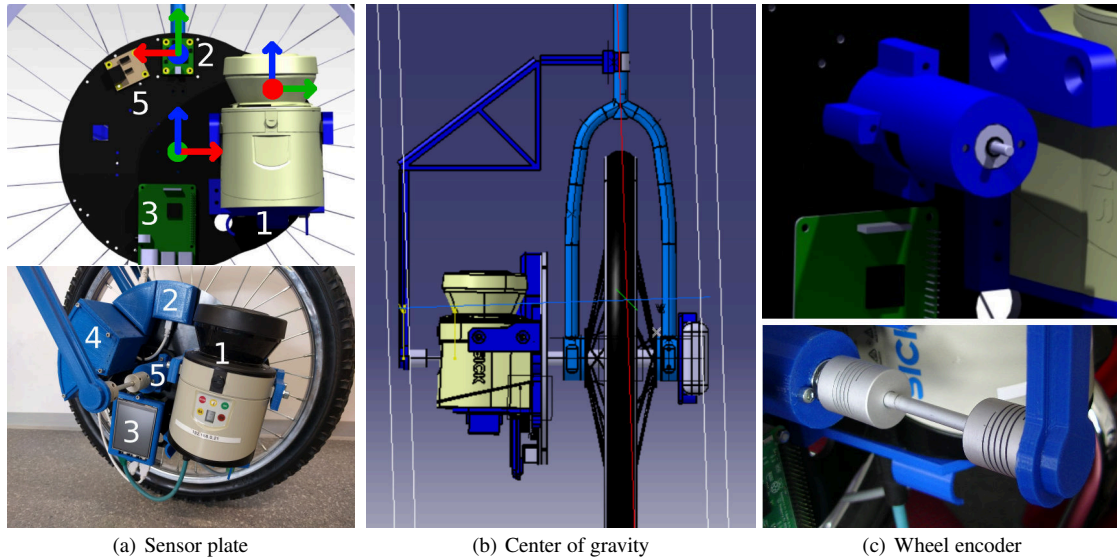
Figure 2. The sensor setup of RADLER. (1) SICK LMS141 LiDAR sensor, (2) PhidgetSpatial Precision 3/3/3 IMU, (3) Raspberry Pi 3 with Display, (4) Cable Box, (5) Phidget optical rotary encoder ISC3004 and encoder high speed.

projection into the xy plane and φ its orientation inside the xy plane. The pitch angle is determined in a similar matter using the y-axis in the global coordinate system as

$$\vartheta = \text{atan2}(\pm q_x, q_z) \text{ with}$$
$$\begin{pmatrix} q_x & q_y & q_z \end{pmatrix} = \boldsymbol{R}_{\mathcal{I} \to \mathcal{G}} \cdot \begin{pmatrix} 0 & 1 & 0 \end{pmatrix}^T. \quad (6)$$

ϑ is used to calibrate the wheel encoder as described in the next section.

The pose of the unicycle is determined with Eq. 2. The rotational part of $T_{\mathcal{U} \to \mathcal{G}}$ is given by $(-\varphi, \vartheta, \psi)$ and the translational part is given by

$$\Delta x_{\mathcal{G}} = \Delta x_{\mathcal{U}} \cdot \cos \psi, \ \Delta y_{\mathcal{G}} = \Delta x_{\mathcal{U}} \cdot \sin \psi, \ \Delta z_{\mathcal{G}} = 0, \quad (7)$$

with $-\varphi$ due to the negative rotation direction of the scanner (see Fig. 2(a)). The initial transformation does not consider any differences in height and is limited by the accuracy of the encoder and the IMU. Algorithmic solutions are necessary to reduce the impact of these limitations. Here the continuous-time SLAM approach from (Elseberg et al., 2013) is used. As this approach is based on the ICP (Iterative Closest Point) algorithm, it benefits from the design of RADLER. The radial rotation allows the 2D laser scanner to measure in front and behind simultaneously, increasing the density and the amount of overlap in the scene.

2.3 Sensor calibration

For accurate odometry, it is important to determine C and L from (3) as precisely as possible. While the circumference of the tire L can be easily measured, the counts per revolution C of the encoder need to be calibrated. In a first attempt C is determined empirically by performing N wheel rotations and dividing the total number of encoder ticks by N. To compensate for systematic errors in the wheel encoder due to environmental influences such as temperature an automatic calibration procedure was developed that can be repeated for each experiment. To this end, Madgwick fused and filtered quaternions from the IMU data are used. Fig. 3 shows an exemplary plot of the calculated angular pitch position of the IMU versus the encoder ticks.
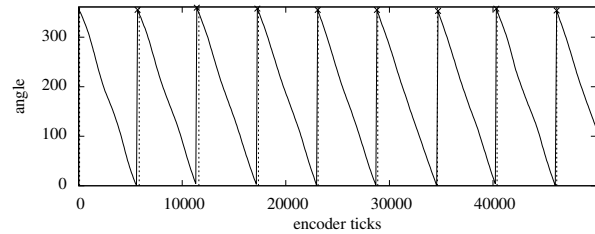

Figure 3. Determination of encoder RPM with IMU data. The continuous line shows the IMU angles, the crosses mark the detected peaks while the dashed lines represent the zero-crossings based on the calibrated encoder.

Detecting peaks in the angular positions allows for calculating the difference in encoder ticks per revolution. These differences are filtered based on the median and then averaged to calculate the number of ticks per revolution. Finally, the offset corresponding to the initial orientation of the encoder is determined. The respective pose of the wheel is then calculated with odometry for movements along the wheel plane and IMU data for the orientation of the wheel as described before.

2.4 Kalman filter

RADLER possesses two sensors for determining the pitch that are prone to different error sources. The wheel encoder is a reliable measurement device, however, the use of a classical unicycle introduces two error sources, the clearance within the main axis and the flexibility of the handle. Enabled by the clearance, the unevenly distributed weight of the laser scanner on the sensor plate causes a small acceleration and deceleration when the center of gravity is shifted towards the front that is not picked up by the encoder. This effect becomes depicted in Figure 4(a). While the pitch $\vartheta_{\mathcal{I}}$ computed from the IMU based on Madgwick fused and filtered quaternions clearly shows a change in slope, the encoder based estimate $\vartheta_{\mathcal{E}}$ shows a linear behavior. Additionally, the frequency of the encoder is significantly lower than the frequency of the IMU measurements with 20 Hz compared to 250 Hz. As the encoder is fixed to the handle, moving the handle up and down distorts the measurements. Thus, the handle needs to be kept in a stable orientation.
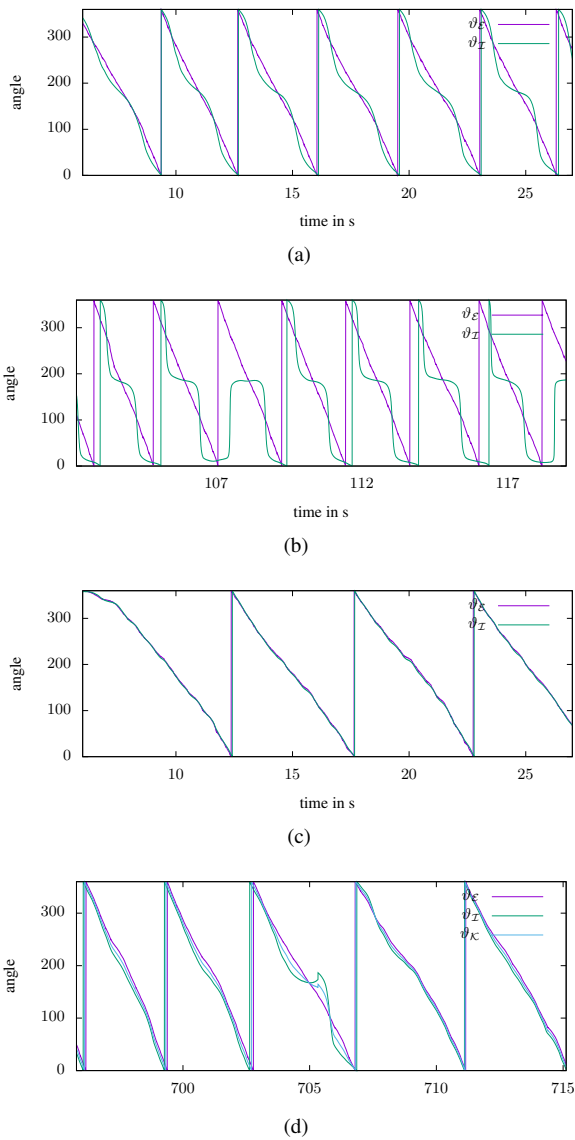
Figure 4. Comparing the pitch computed from encoder $\vartheta_{\mathcal{E}}$, IMU $\vartheta_{\mathcal{I}}$ and fused using a Kalman filter $\vartheta_{\mathcal{K}}$.

IMUs are known to drift and especially low-cost IMUs typically feature significant noise and are easily influenced by environmental disturbances. While the main drift appears in the yaw direction of the unicycle, occasional inaccuracies in detecting the main rotation axis may lead to a misdetection of the pitch angle as shown in Figure 4(b).

To improve the accuracy of the odometry a Kalman filter was implemented for sensor fusion of IMU and wheel encoder. To overcome the frequency limitation of the encoder a linear interpolation into the future is performed for each IMU measurement $\vartheta_{\mathcal{I}}$. The co-variances for both measurements are chosen as $\Sigma_{\vartheta_{\mathcal{I}}} = \Sigma_{\vartheta_{\mathcal{E}}=1}$. Figure 4(d) shows exemplarily the filtering results. A slower motion (cf. Figure 4(c) and 4(a)) reduces the distance error between the two computations. The Kalman filter combines the data by smoothing out the steps from the low frequency encoder measurements, and reduces effects from the clearance within the main axis as well as temporary glitches from the noise in the IMU data.
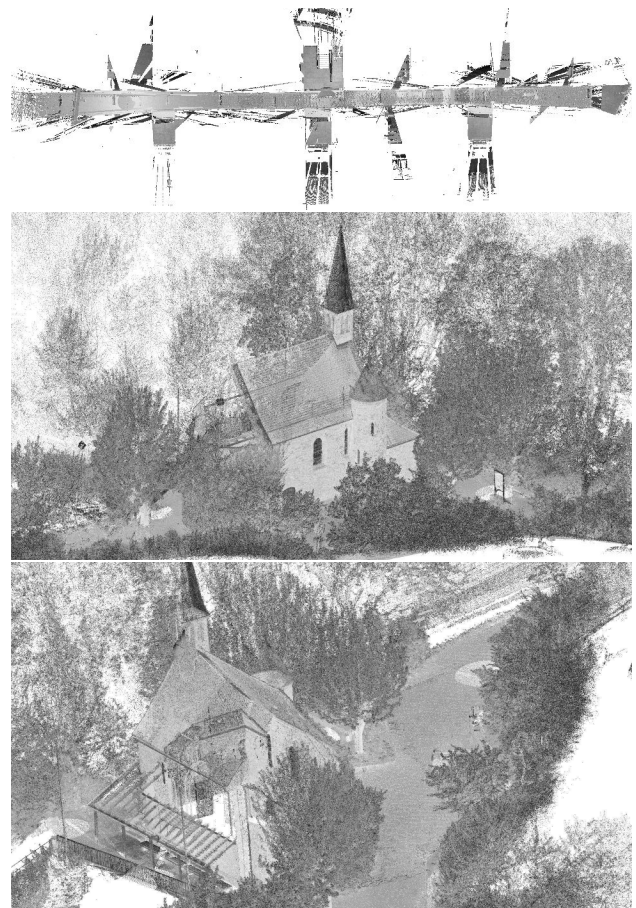

Figure 5. Ground truth data acquired with a Riegl VZ-400 terrestrial laser scanner. Top view from "The Hallway" and two perspectives from "The Chapel". The Grey values represent the reflectance of the materials.

3. EXPERIMENTAL RESULTS

To evaluate the performance of RADLER, four test scenarios in different environments were performed. The first and second experiments were conducted on the 1st floor of the University of Würzburg's computer science ("The Hallway") and old mathematics building ("The Circle"), respectively. Two outside experiments took place at the Maria-Schmerz-Chapel[2] ("The Chapel") and the Old Main Bridge [3], Würzburg's oldest bridge across the river Main ("The Bridge"). Scans obtained with a Riegl VZ-400 laser scanner serve as ground truth for "The Hallway", "The Chapel" and "The Bridge".

1. "The Hallway" Being the simplest movement consisting of a straight line over approximately 200 m on a smooth surface with no slope. The data set acquired with a scanning frequency of 50 Hz and a resolution of 0.5 ° results in around 3.5 million points. Typically for an office building, the hallway consists of multiple doors and glass facades, yielding problems for laser scanners due to reflections and ghost projections (partly visible in Fig. 5 (top) and Fig. 6 (top)).

2. "The Circle" Again, the surface was smooth without slope, a full circle there and back again was conducted for this

---

[2] http://www.wuerzburgwiki.de/wiki/Maria-Schmerz-Kapelle_(Randersacker)

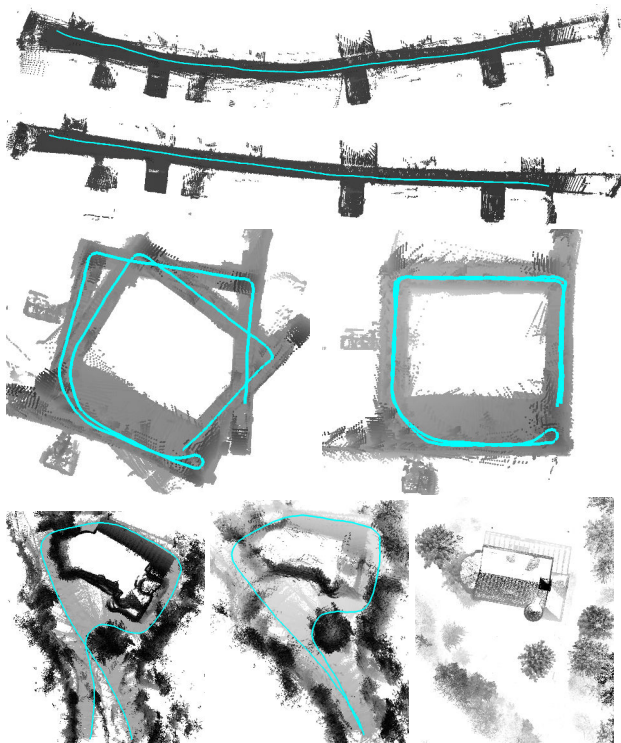[3] https://wuerzburgwiki.de/wiki/Alte_Mainbrücke

Figure 6. Topview showing the results from the experiments one to three: first, the initial trajectory, second, the results from the continuous-time SLAM algorithm. From top to bottom: "The Hallway","The Circle" and "The Chapel". The noisy appearance of the indoor data sets results from reflecting surfaces such as glass. The initial trajectory of "The Chapel" data set is planar. After correction, the true 3D structure of the surface becomes clear when looking at the shading. As the chapel is lower than the starting position the shading by height has less impact on the roof of the chapel which is therefore lighter in color. The third image shows the reference data set collected with a Riegl VZ-400 laser scanner.

experiment to compensate the limited field of view of the unicycle. The IMU drift is strongly present, but was removed by the continuous-time SLAM. The full data set results in around 6.3 million points.

3. "The Chapel" being the first of the two outdoor data sets, is also more challenging with a gravel-like surface and slopes. Starting at the highest point and descending to the level surroundings of the chapel, a final ascend back to the starting point was done. Since the initial trajectory was only 2D, the differences in elevation were corrected using the SLAM algorithm and the global consistency was improved. The data set consists of around 3.5 million points.

4. "The Bridge" with around 4 million points, was selected to evaluate the final 3D model. The Old Main Bridge has a length of about 185 m and is completely made from stone. Twelve statues of saints are placed on the bridge, six on each side. The floor is made of cobblestone and slightly curved upwards from one side to the other. The recorded trajectory goes there and back again to record both sides in a closed loop. For this experiment a scanning frequency of 25 Hz and a resolution of $0.25°$ was chosen. To compensate for the lower frequency the walking speed was decreased as seen in Figure 4. Eight reference scans were taken with an angular resolution of $0.04°$
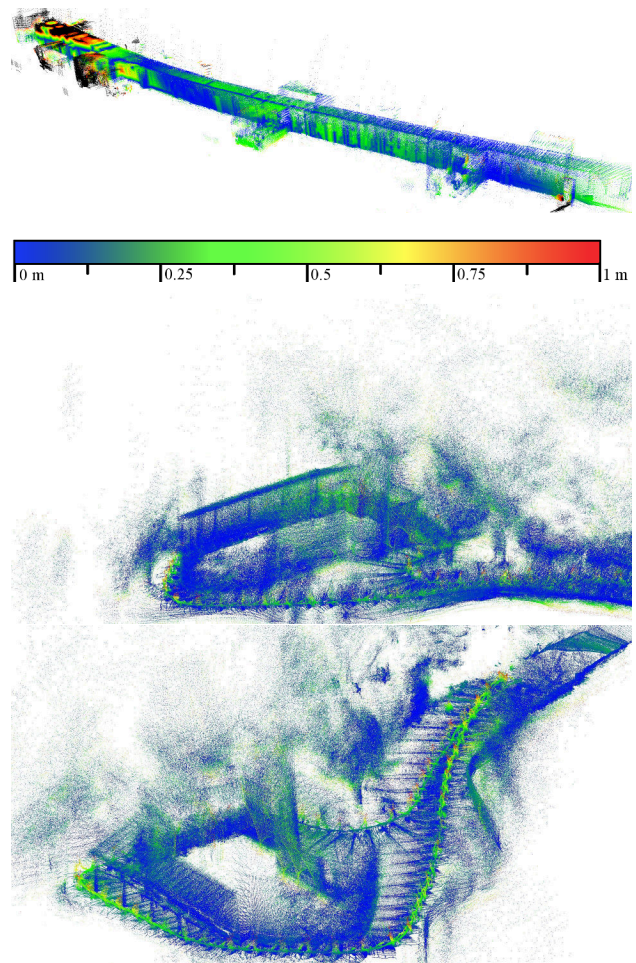

Figure 7. Registered point clouds for "The Hallway" and two perspectives from "The Chapel", respective to Fig. 5. The color represents the shown scale, ranging from 0 m (blue) to 1 m (red) point-to-point distance.

An evaluation of the simple calibration method in comparison to the automatic calibration reveals that the encoder produces data at a resolution of $\approx \, ^1/_{16}°$ for all data sets, attenuating the assumption of susceptibility to environmental influences. Fig. 5 shows the Riegl scans from "The Hallway" as a top view and "The Chapel" from two different sides. The gray values of the points represent the reflectance of the materials. The results shown in Fig. 7 were obtained after about 150 iterations of the continuous time-SLAM algorithm. To calculate the point-to-point distance, the RADLER data was first matched to the ground truth using the ICP algorithm, implemented in 3DTK (Nüchter et al., 2018). The points are colored with the point-to-point distance on the shown color scale, ranging from 0 m to 1 m.

"The Hallway" compares well to the ground truth, especially in the first three quarters of the way from right to left in Fig. 7 (top). Black color marks points with a point-to-point distance greater than 1 m. They almost exclusively appear in the last quarter, which is a result of the large glass front at the end of "The Hallway". RADLER scans mostly towards one side causing one wall to be sparsely covered. Without loop closure, the ICP algorithm would contract the data towards one side and thus bend the trajectory.

Fig. 6 shows top views of the last two experiments with the originally obtained trajectory as well as the improved trajectory
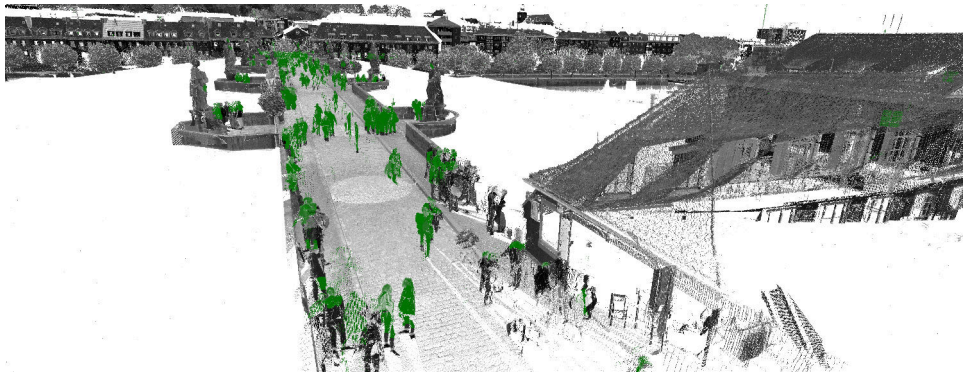
Figure 8. Ground truth of "The Bridge'. The Grey values represent the reflectance of the materials. Green points are dynamic objects, detected and removed with the *peopleremover* (Schauer and Nüchter, 2018).

after few iterations of the continuous-time SLAM. The closed loop helps to improve the trajectory significantly, compared to the previously mentioned deviation for "The Hallway". Having a longer trajectory, "The Circle" still converges nicely to the rectangular shape of the building. Blurry edges in the top view show the necessity of further improvements in calibration. For longer trajectories a single offset and static RPM values appear not to be sufficient.

"The Chapel" also compares well to the ground truth with less outliers compared to 'The Hallway'. Though the rough terrain does not seem to influence the quality of the output in a negative way, the closed loop within the path made a proper correction of the trajectory with the continuous-time SLAM algorithm possible. The major drawback in the outdoor scene comes from the limited range of the laser scanner and the lower density at increasing distances. The roof of the chapel is also hardly covered by points. To increase the density, the unicycle could be moved much slower than in the current experiments or the trajectory could be followed twice. It would also be an option to exchange the LMS141 for a model with a greater maximum measuring distance, but this would increase the cost of the hardware drastically.

Eliminating the drawbacks identified in the previous experiments "The Bridge" provides a clear view on the performance of our approach. Fig. 8 shows the ground truth. The statues of the saints and the opposing riverbanks are clearly visible. Green points are dynamic objects, detected and removed with the *peopleremover* (Schauer and Nüchter, 2018). Since RADLERs laser scanner has limited range compared to the Riegl scanner, the surroundings are cut off for further comparison.

Fig. 9 shows a top view of "The Bridge". Fig. 9(a) shows the ground truth, Fig. 9(b) the final trajectory of RADLER after about 100 iterations of the continuous-time SLAM algorithm and Fig. 9(c) how the point cloud was corrected. The final point cloud was registered into the coordinate system of the ground truth using the ICP implementation from (Nüchter et al., 2018). Similar to all previous experiments, the initial trajectory shows a drift relative to the actual path. Although the turning point is well recorded, the curvature to the right causes start and end of the trajectory to not meet, which was also fixed by the continuous-time SLAM algorithm. The length of the bridge was accurately recorded, as can be seen when looking at the statues of saints and the houses near the end of the bridge. Challenging however is the change in altitude and the resulting upwards curvature of the bridge. The initial point cloud (Fig. 10, top) does not show any upwards curvature as a result

of the initial orientation of RADLER, which leads to a distance of several meters at the end of the bridge to the ground truth. As is clearly visible in Fig. 10, bottom, in the middle of the bridge the final point cloud lies about 30 cm above, at the beginning (right) and end (left) of the trajectory about 2 m and 4 m, respectively, below the reference data. This overcompensation of the curvature may be a result of the mounting position of the laser scanner. Since the scanners distance to the ground varies between 0.1 m and 0.4 m due to its off center placement and the minimal measuring distance of the scanner is 0.5 m, the laser arrays measuring the ground have a very small incident angle, which yields a large measuring area per array. This leads to false measurements combined with systematic errors for all points close to the ground. These observations are supported by the quantitative analysis of Fig. 11. While the floor at the end of the bridge deviates from the ground truth by about 4 m, the rail deviates by about 30 cm less, as is visible by the color gradient. The correct length of the bridge is visible when looking at the color of the statues, which shows little to no errors. A closer look at one of the statues is given in 12. Although the point cloud is sparse and the scattered points make it impossible to inspect any details, the statue is clearly recognizable as such, as is the bench. In the lower areas, the statue and the bushes show point-to-point errors below 10 cm, where the higher areas show larger errors, some even above 50 cm. This is due to larger distances yielding larger errors. When looking at Fig. 10 it is visible, that the continuous-time SLAM algorithm, despite the clear errors in the initial trajectory, was able to create a dense, albeit noisy point cloud.

Computing the initial trajectory by fusing IMU and encoder data leads to higher accuracy in the final point cloud. In Figure 10 the curvature of the bridge is better represented. This results most likely from the compensation of the error introduced by the clearance within the main axis. This becomes also evident when looking at the point-to-point distances in Figure 11. The error towards the sides is reduced to less than a meter. In the close-up view the statue becomes more pronounced and no points surpass the 0.5 m limit of the color scale.

4. CONCLUSIONS

This paper presents a new, low-cost way of generating 3D point clouds without the utilization of a classical 3D laser scanner. A modified unicycle with a 3D laser profiler, an IMU and a wheel encoder was used to generate 3D point clouds and the results were optimized using our continuous-time SLAM algorithm. The experiments and the discussion show, that the
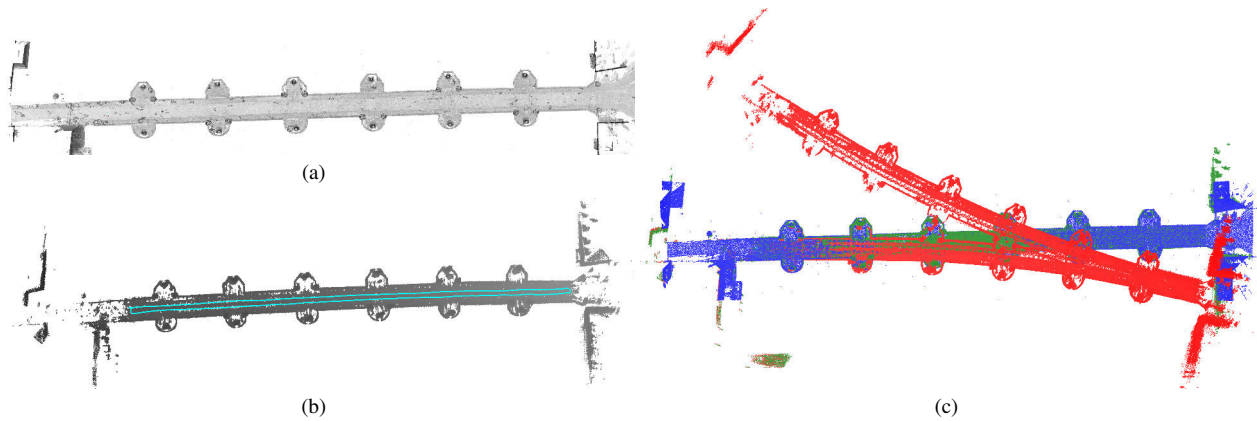
Figure 9. Topview of "The Bridge". 9(a) Ground truth only showing the bridge, not the surroundings. 9(b) Final trajectory, created with the continuous-time SLAM. 9(c) Reference data (blue) with overlaid initial (red) and final (green) RADLER point cloud.
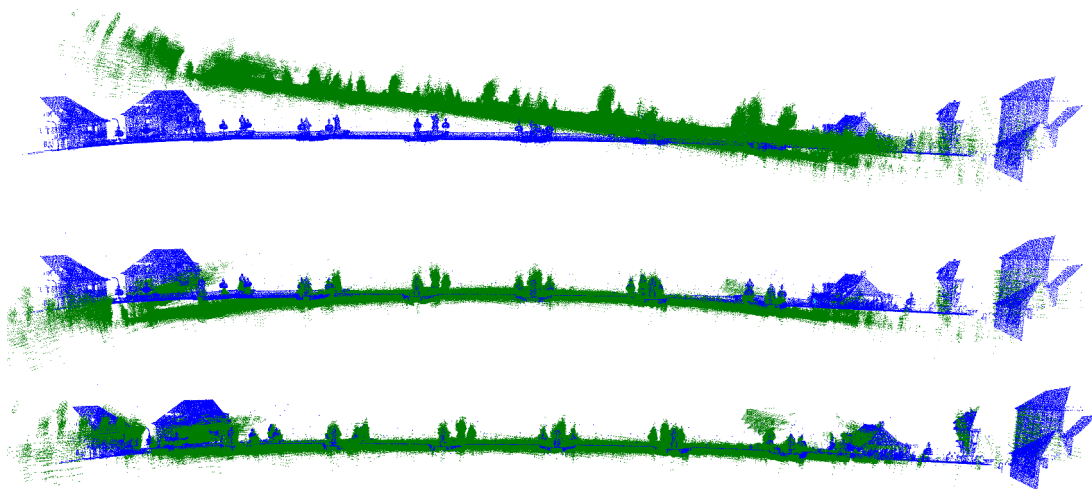

Figure 10. Sideview of "The Bridge". Initial (top) and final point cloud without (center) and with Kalman filter initialization (bottom) compared to ground truth (blue). The final point clouds were registered with the ICP implementation from (Nüchter et al., 2018).

results are already promising and meaningful 3D point clouds are generated. Fusing the data from both rotation sensors using a Kalman filter leads to improved accuracy. Ideal use cases for RADLER are surveying and mapping in small, narrow areas where precise reconstruction of small features is not the main objective. Measuring the inside of a building to reconstruct the floor plan, creating a BIM (Building Information Model) or create 3D models of old city centers or historical buildings, which often only have narrow, steep and hardly accessible streets or hallways, predestined for mobile laser scanning, come to mind. Typical errors lie within a range of 0 cm to 20 cm, which account for 68.1 % of all errors of "The Bridge" with a Kalman filtered initial trajectory, while only 32.0 % of errors lie within that range when not using a Kalman filter. Especially challenging remains the precise reconstruction of elevation profiles, which is due to the aforementioned mounting of the scanner close to the ground. However, the fusion of IMU and encoder measurements leads to improved initial trajectories, reducing errors from several meters at the edge of the scans to less than a meter. But needless to say, a lot of work remains to be done. In the future, we plan to integrate a GNSS device to provide a better initial trajectory for the continuous-time SLAM algorithm. Also, the mounting system of the sensors needs to be improved in order to overcome the drawbacks a classical unicycle provides, such as the clearance within the main axis.

REFERENCES

Borrmann, D., Jörissen, S., Nüchter, A., 2018. RADLER - A RADial LasER scanning device. *Proceedings of the 16th International Symposium of Experimental Robotics (ISER '18)*, Springer Tracts in Advanced Robotics, Buenos Aires, Argentina, 655–664.

Bosse, M., Zlot, R., Flick, P., 2012. Zebedee: Design of a spring-mounted 3-d range sensor with application to mobile mapping. *Robotics, IEEE Transactions on*, 28(5), 1104–1119.

Elseberg, J., Borrmann, D., Nüchter, A., 2013. Algorithmic Solutions for Computing Precise Maximum Likelihood 3D Point Clouds from Mobile Laser Scanning Platforms. *Remote Sensing*, 5(11), 5871–5906.

Frederic Lardinois, TC, 2015. Google Unveils The Cartographer, Its Indoor Mapping Backpack. `https://techcrunch`
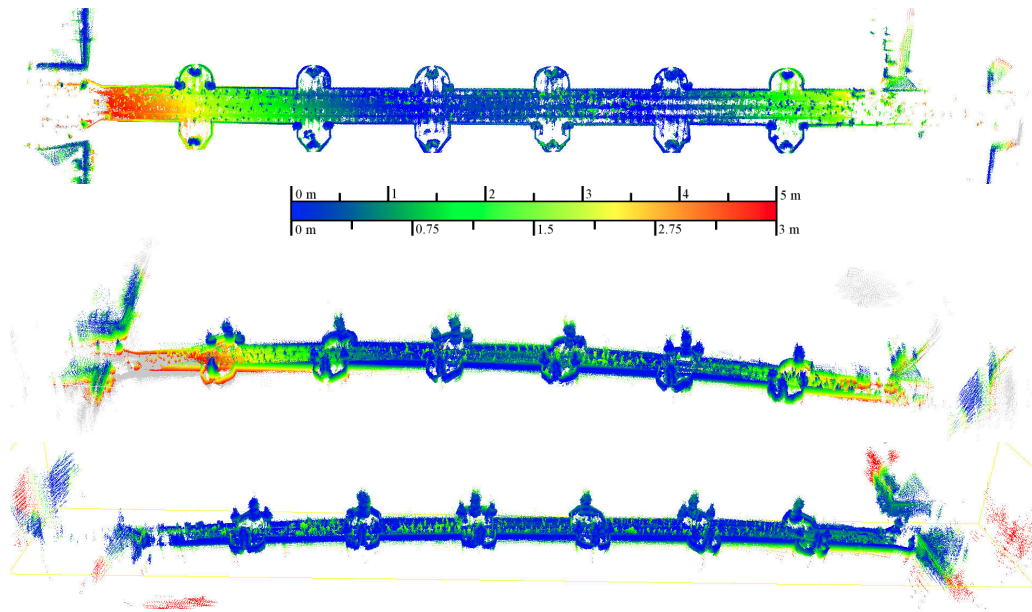
Figure 11. Final point clouds of "The Bridge" as topview (top) and sideview. The sideview is shown without (above) and with (below) the initialization using the Kalman filter. The colors show the point-to-point distance respective to the presented color scale. The topview has a gradient from 0 m (blue) to 5 m (red), where as the sideview only goes to 3 m to make details in the middle of the bridge more distinguishable. Grey points have a point-to-point distance outside of that range.
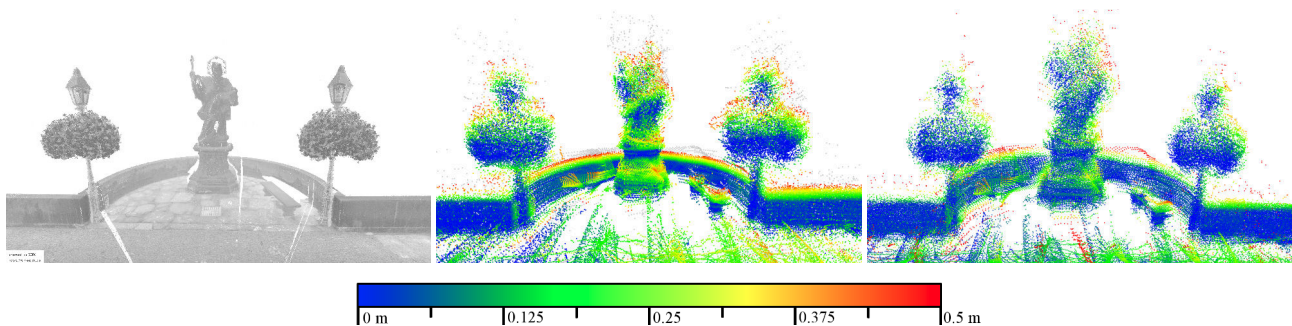

Figure 12. A closer look at the bridge saint *John of Nepomuk* , third from left in Fig. 11 (top). Left: reference data from the Riegl VZ-400 laser scanner. Center: final point cloud of RADLER. Right: final point cloud using the Kalman filter. The color shows the point-to-point distance respective to the provided color gradient from 0 m to 0.5 m.

.com/2014/09/04/google-unveils-the-cartographer-its-indoor-mapping-backpack/.

Google, 2015. Street View Trolley. http://maps.google.com/intl/en/maps/about/behind-the-scenes/streetview.

Lauterbach, H. A., Borrmann, D., Hess, R., Eck, D., Schilling, K., Nüchter, A., 2015. Evaluation of a Backpack-Mounted 3D Mobile Scanning System. *Remote Sensing*, 7(10), 13753-13781.

Lehtola, V. V., Virtanen, J.-P., Kukko, A., Kaartinen, H., Hyyppä, H., 2015. Localization of mobile laser scanner using classical mechanics. *ISPRS Journal of Photogrammetry and Remote Sensing*, 99, 25–29.

Lehtola, V. V., Virtanen, J.-P., Vaaja, M. T., Hyyppä, H., Nüchter, A., 2016. Localization of a mobile laser scanner via dimensional reduction. *ISPRS Journal of Photogrammetry and Remote Sensing*, 121, 48-59.

Leica, 2015. Leica pegasus:backpack. www.leica-geosystems.com/de/Leica-PegasusBackpack_106730.htm.

NavVis, 2015. M3 trolley. https://www.navvis.com/explore/trolley/.

Nüchter, A., Elseberg, J., Borrmann, D., 2013. Irma3D – An Intelligent Robot for Mapping Applications. *Proceedings of the 3rd IFAC Symposium on Telematics Applications (TA '13)*, Seoul, Korea, 119–124.

Nüchter, A. et al., 2018. 3DTK — The 3D Toolkit. http://threedtk.de/.

Schauer, J., Nüchter, A., 2018. The Peopleremover — Removing Dynamic Objects From 3-D Point Cloud Data by Traversing a Voxel Occupancy Grid. *IEEE Robotics and Automation Letters (RAL)*, 3(3), 1679–1686. https://robotik.informatik.uni-wuerzburg.de/telematics/download/icra2018.pdf.

Thomson, C., Apostolopoulos, G., Backes, D., Boehm, J., 2013. Mobile Laser Scanning for Indoor Modelling. *ISPRS Annals of Photogrammetry, Remote Sensing and Spatial Information Sciences*, II-5/W2, 289–293.

VIAmetris, 2015. Mobile Mapping Technology. http://www.viametris.com/.